Homoclinic orbits in three-dimensional Shilnikov-type chaotic systems*

Feng Jing-Jing(冯晶晶)[a)b)c)], Zhang Qi-Chang(张琪昌)[a)b)], Wang Wei(王 炜)[a)b)†], and Hao Shu-Ying(郝淑英)[c)]

[a)] *Tianjin Key Labortory of Nonlinear Dynamics and Chaos Control, School of Mechanical Engineering, Tianjin University, Tianjin* 300072, *China*

[b)] *State Key Laboratory of Engines, Tianjin University, Tianjin* 300072, *China*

[c)] *School of Mechanical Engineering, Tianjin University of Technology, Tianjin* 300384, *China*

(Received 15 November 2012; revised manuscript received 20 March 2013)

In this paper, the Padé approximant and analytic solution in the neighborhood of the initial value are introduced into the process of constructing the Shilnikov type homoclinic trajectories in three-dimensional nonlinear dynamical systems. The PID controller system with quadratic and cubic nonlinearities, the simplified solar-wind-driven-magnetosphere-ionosphere system, and the human DNA sequence system are considered. With the aid of presenting a new condition, the solutions of solving the boundary-value problems which are formulated for the trajectory and evaluating the initial amplitude values become available. At the same time, the value of the bifurcation parameter is obtained directly, which is almost consistent with the numerical result.

Keywords: chaos, Shilnikov theorem, homoclinic orbit, Padé approximation

PACS: 05.45.Gg, 02.30.Oz **DOI:** 10.1088/1674-1056/22/9/090503

1. Introduction

Bifurcation and chaos of three-dimensional (3D) systems are always the core research content of the complex dynamical behavior in nonlinear systems. The study of chaos has achieved quite great progress since Lorenz[1] found the first chaotic attractor in 1963. After that, many continuous-time autonomous quadratic chaotic systems have been found, such as the modified Lorenz system,[2] the Rössler system,[3] the Chen system,[4] and so on. The homoclinic orbits are of great importance for theoretical study and practical applications, and lots of papers dealing with this subject have been published.[5–8] For instance, Leonov[9] used frequency estimates to obtain upper bounds of the Lyapunov dimension of attractors and proved the existence of homoclinic orbits in Lorenz system. Li *et al.*[10] proved the existence of homoclinic and heteroclinic orbits in the modified Lorenz system by expressing the solution in power series and finding some parameters. Genesio *et al.*[11] pointed out the main complex dynamics that can be exhibited and gave indications, which can predict possible homoclinic orbits in a Rössler system.

In our research, the Shilnikov homoclinic and heteroclinic theorems[12] are important analytical methods for chaotic motion in 3D nonlinear dynamical systems. It is possible to prove the existence of chaos in 3D continuous dynamical systems by providing analytical criteria, and subsequently to determine the strange attractor in those systems. According to the application of the Shilnikov theorem, on the one hand, the derivative range of the chaotic motion is found which aims to ensure the timing of strange attractors existence. On the other hand, those simple chaotic systems with a rich dynamical behavior based on the requirements of the theorem are constructed. Palmer[13] applied the shadowing lemma and proved the Shilnikov theorem in strict mathematics, which is a stochastic research direction. Zhang *et al.*[14] analyzed the properties of mechanically and electrically coupled nonlinear dynamical systems which are based on the Shilnikov criterion and presented a rigorous proof of the existence of horseshoe chaos. Zhou *et al.*[15] constructed a new 3D chaotic system of quadratic polynomial ordinary differential equations with a single equilibrium point and demonstrated the evolution process from flip bifurcation to chaos by numerical simulation.

However, it mainly relies on visual aspects to find the chaotic attractor by numerical calculation with great contingency, during which it is time-consuming to find the bifurcation parameter values and the location of the initial point. Therefore, it is necessary to find a simple and effective analytical method for constructing the homoclinic orbit expressions of 3D systems. The existing methods are mostly used for a simple quadratic autonomous chaotic system, and the specific analytical expressions of the Shilnikov type homoclinic orbits are rarely given. Mikhlin[16] used a quasi-Padé approximant

*Project supported by the National Natural Science Foundation of China (Grant Nos. 11072168 and 11102127), the Specialized Research Fund for the Doctoral Program of Higher Education of China (Grant No. 20100032120006), and the Research Program of Application Foundation and Advanced Technology of Tianjin, China (Grant Nos. 12JCYBJC12500 and 11JCYBJC05800).

†Corresponding author. E-mail: wangweifrancis@tju.edu.cn

© 2013 Chinese Physical Society and IOP Publishing Ltd

method to construct homoclinic orbits of the Lorenz equation. Vakakis and Azeez[17] expressed the solution in power series such as $t \to \pm 0$ and introduced global approximants to match the local solutions by means of a Padé-like procedure. According to the characteristics of a n-dimensional quadratic system, Li and Zhu.[18] constructed the s-dimensional series expression of the stable and unstable manifolds, which formed a homoclinic orbit near the hyperbolic singular point of the Lorenz system. Nandakumar and Chatterjee.[19] used splines in phase space to construct the continuation of limit cycles near saddle homoclinic points in the Lorenz system and Chua's circuit. Chen *et al.*[20] used the undetermined coefficient method to derive the analytic expression of a relevant degenerate homoclinic orbit. One of the three eigenvalues of the Jacobian was evaluated to be zero at an equilibrium point, and the other two were found to form a pair of conjugate complex numbers.

The Padé approximants were successfully used for the homoclinic orbits of two-dimensional (2D) axisymmetric breathers by Emaci *et al.*[21] Quasi-Padé approximants were used to construct the homoclinic orbits in a nonlinear Schrödinger equation system by Manucharyan and Mikhlin.[22] Analytic homoclinic orbits in the non-autonomous Duffing equation and the van der Pol–Duffing equation with weakly coupled nonlinear oscillators were computed by Mikhlin.[23] The Padé approximation[24,25] was extended to generate the solutions which satisfied the boundary-value of homoclinic and heteroclinic solutions, and then to derive the critical values of bifurcation in the corresponding conservative, autonomous and non-autonomous systems with quadratic and cubic nonlinear oscillators, and the system parameters of the linear and nonlinear terms were variable. Moreover, Zhang *et al.*[24] constructed the homoclinic and heteroclinic orbits in general asymmetric double well and triple well systems to improve the accuracy of the threshold for the onset of chaos.

In this paper, we present a completely analytic framework of how to find homoclinic orbits and bifurcation parameter in a 3D autonomous nonlinear system that is Shilnikov sense Smale horseshoe chaos. The values of bifurcation parameter and initial position of the point are obtained directly according to the calculation in which the Padé approximation method is introduced and the analytic solution in the neighbourhood of initial value; besides the analytical expressions of the Shilnikov type homoclinic orbits are formed. The values of bifurcation parameter obtained using the method presented in this paper are almost identical with the numerical results, by contrast, those values obtained by the Shilnikov theorem are far from accurate.

The rest of this paper is organized as follows. In Section 2, the arguments for the introduction of new conditions are presented. In Section 3, the calculation procedures of the presented method in this paper are introduced. In Section 4, examples of the Shilnikov sense Smale horseshoe chaotic problems of a modified PID controller 3D system, a simplified WINDMI (solar wind driven magnetosphere ionosphere) model, and a human NDA sequences model are discussed. The final section, i.e., Section 5, is devoted to some conclusions drawn from the present study.

2. Method demonstration

In the construction of the homoclinic and heteroclinic orbits in nonlinear dynamical systems, numerical simulations are used in most cases, while the analytical approaches are rarely given. The expressions of homoclinic and heteroclinic orbits are more difficult to find in 3D systems or high-dimensional systems.

Based on the series expression method considering the radius of convergence,[18] the analytic expression of the Shilnikov type homoclinic orbit is accomplished in Ref. [26]. Figures 1 and 2 show the 3D phase diagram and the time series of trajectory $x(t)$, $y(t)$, and $z(t)$, where t_x, t_y, and t_z are the time point when the trajectory $x(t)$, $y(t)$, and $z(t)$ intersect between positive direction ($t \to +\infty$) and negative direction ($t \to -\infty$) respectively. As can be seen in the Figures, in system I, t_x and t_z are almost coincident, but t_y does not appear. It means that the trajectories $x(t)$ and $z(t)$ can intersect at the same time but the trajectory $y(t)$

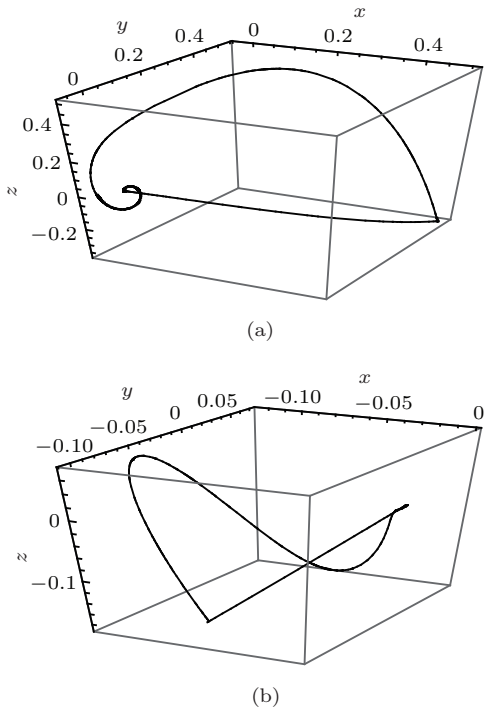


Fig. 1. The 3D phase diagrams: (a) system I, (b) system II.

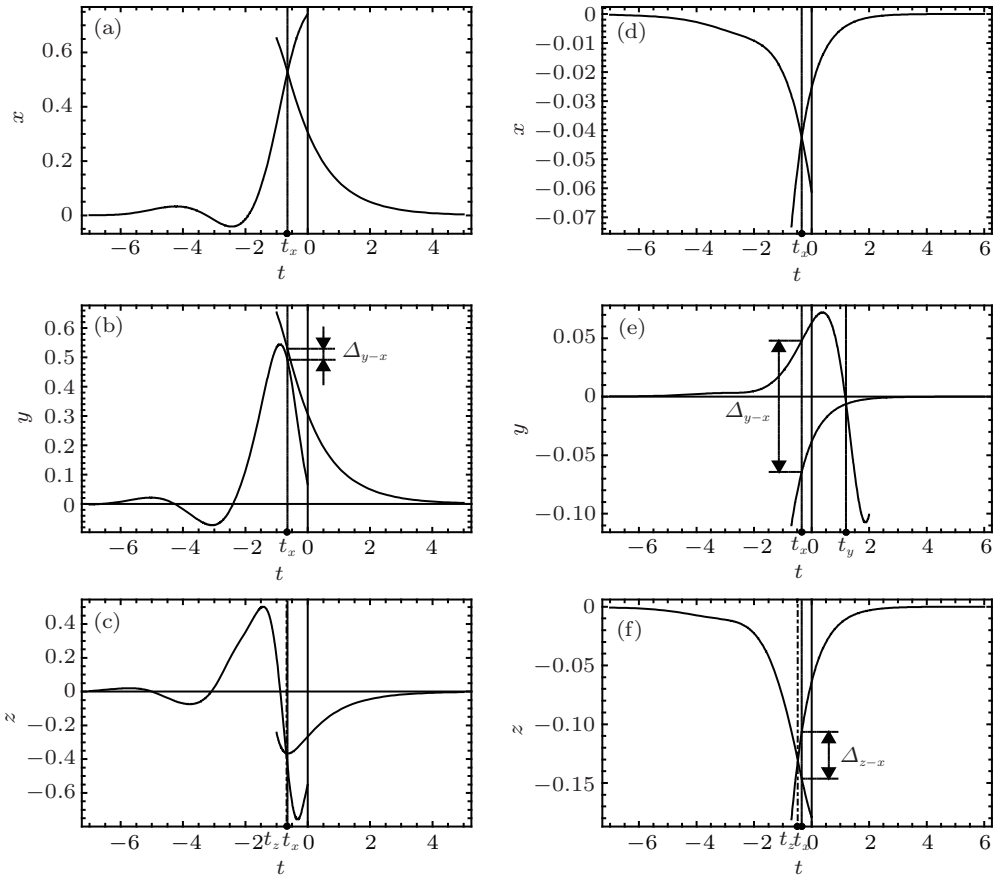


Fig. 2. Time series of trajectories of (a) $x(t)$, (b) $y(t)$, and (c) $z(t)$ of system I; (d) $x(t)$, (e) $y(t)$, and (f) $z(t)$ of system II.

does not intersect between the positive direction and the negative direction. Δ_{y-x} is the distance of trajectory $y(t)$ between the positive direction and the negative direction at moment t_x. In system II, t_x and t_z are very close to each other, but t_y is far from both of them. Δ_{y-x} and Δ_{z-x} are the distances of trajectories $y(t)$ and $z(t)$ between the positive direction and the negative direction at t_x. In other words, the point which is the farthest from the saddle point in the phase diagram does not exist on the curve at which the trajectories $x(t)$, $y(t)$, and $z(t)$ between positive direction and negative direction intersect at the same time. In summary, the three solutions cannot intersect at the same point at the same time.

The homoclinic orbits are defined as trajectories which arrive at the same singular point when $t \to +\infty$ and $t \to -\infty$, namely the curves are connected at the same saddle point. It means that when we use the approximate method to solve the homoclnic orbit of a system the orbit is required to be a complete smooth curve, and the beginning and end of the orbit should cross the same saddle point, or at least very close to the saddle point (as there might be some errors in the approximate calculation). And rupture of homoclinic orbits can lead to occurrence of chaotic phenomena. The variations process from a homoclinic orbit to chaos can be described as shown in Fig. 3.

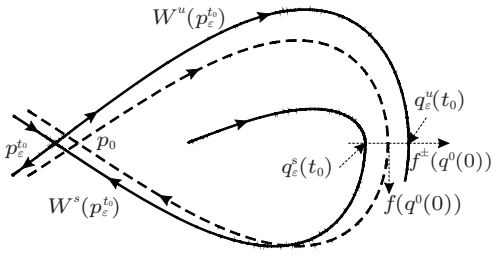


Fig. 3. Rupture process of a homoclinic orbit.

When considering the accuracy problem of the existing method, other approximate methods that can solve the accuracy problem need to be found. This ensures that the obtained analytical homoclinic orbit meets the natural properties, which should be a smooth and closed orbit through or near the saddle point. In this paper, the Padé approximation method and analytic solution in the neighborhood of the initial value are considered to solve the issue that the manifolds in $x(t)$, $y(t)$, and $z(t)$ directions, come from the saddle. The peak of homoclinic solutions can intersect at one point at the same time, and simultaneously the values of bifurcation parameter can be obtained directly when the system has homoclinic orbits. The range of values is more accurate than the one determined by the Shilnikov method. The specific calculation process is explained in the next section.

3. Framework of finding homoclinic orbits

3.1. Characterization analysis

In this section, a framework of finding possible homoclinic orbits in a 3D autonomous nonlinear system is presented. Assume that the normal form of this system is

$$\frac{\mathrm{d}Z}{\mathrm{d}t} = AZ + o(2), \tag{1}$$

where $Z = (x, y, z)^{\mathrm{T}}$, and the corresponding Jacobian matrices evaluated at the origin are

$$A = \begin{pmatrix} \lambda_1 & & \\ & \lambda_2 & \\ & & \lambda_3 \end{pmatrix}. \tag{2}$$

Without loss of generality, assume that matrix (2) has one real root and a conjugate pair of complex roots, where the real root is negative and the real part of the complex conjugate roots is positive. According to the above conditions, we define that h, g, $f \in \Re$, $h > 0$, $g > 0$, $f > 0$. A negative real root and a pair of positive real parts of the conjugate complex roots are obtained as follows:

$$\begin{aligned} \lambda_1 &= -h, \\ \lambda_{2,3} &= g \pm \mathrm{i}f. \end{aligned} \tag{3}$$

The calculation procedure of the matrix that has a positive real root and a pair of negative real parts of the conjugate complex roots is similar to the process described below.

3.2. Local expansion of the homoclinic solution

Since the calculation process is complicated and time-consuming in many systems when using the invariant manifold theorem to calculate the stable and unstable manifold equation, series expressions of the stable and unstable manifolds at a hyperbolic saddle-focus point by taking the one-dimensional (1D) manifolds and 2D manifolds into consideration in calculation are introduced. The 1D manifold in Eq. (1) can be expressed as

$$\begin{aligned} x^{[+]}(t) &= \sum_{k=0}^{n} a_k \mathrm{e}^{k\lambda_1 t}, \\ y^{[+]}(t) &= \sum_{k=0}^{n} b_k \mathrm{e}^{k\lambda_1 t}, \\ y^{[+]}(t) &= \sum_{k=0}^{n} c_k \mathrm{e}^{k\lambda_1 t}, (t \to +\infty), \end{aligned} \tag{4}$$

where a_k, b_k, and c_k are undetermined coefficients.

Similarly, the 2D manifold expressions in the equation are

$$\begin{aligned} x^{[-]}(t) &= \sum_{k=0}^{n} \sum_{j=0}^{n-k} a_{k,j} \mathrm{e}^{k\lambda_2 t + j\lambda_3 t}, \\ y^{[-]}(t) &= \sum_{k=0}^{n} \sum_{j=0}^{n-k} b_{k,j} \mathrm{e}^{k\lambda_2 t + j\lambda_3 t}, \\ y^{[-]}(t) &= \sum_{k=0}^{n} \sum_{j=0}^{n-k} c_{k,j} \mathrm{e}^{k\lambda_2 t + j\lambda_3 t}, \ (t \to -\infty), \end{aligned} \tag{5}$$

where $a_{k,j}$, $b_{k,j}$, and $c_{k,j}$ are undetermined coefficients as before.

Here, analytic solutions in the neighborhood of the initial value are considered to eliminate the disjoint problem between 1D and 2D manifold expressions in traditional algorithms. The relations between 1D and 2D manifold expressions are strengthened. Since the homoclinic solution is analytic in the neighborhood of $t = 0$, the solution in power series as $t \to \pm 0$ can be expressed as follows:

$$\begin{aligned} x^{[0]}(t) &= \sum_{k=0} x_k^{[0]} t^k, \\ y^{[0]}(t) &= \sum_{k=0} y_k^{[0]} t^k, \\ z^{[0]}(t) &= \sum_{k=0} z_k^{[0]} t^k, \ (t \to \pm 0). \end{aligned} \tag{6}$$

Substituting Eq. (6) into Eq. (1) and matching coefficients of respective powers of t, we obtain the recursive expressions represented by constant coefficients of series as follows:

$$\begin{aligned} x_{k+1}^{[0]} &= \frac{1}{k+1}[\lambda_1 x_k^{[0]} + o(2)], \\ y_{k+1}^{[0]} &= \frac{1}{k+1}[\lambda_2 y_k^{[0]} + o(2)], \\ z_{k+1}^{[0]} &= \frac{1}{k+1}[\lambda_3 z_k^{[0]} + o(2)]. \end{aligned} \tag{7}$$

Since system (1) is autonomous, the selected initial conditions of the orbit can arbitrarily be at the point where $x(0) = x_0$, $y(0) = y_0$, and $\dot{z}(0) = 0$. Thus,

$$\begin{aligned} x_0^{[0]} &= x_0, \\ y_0^{[0]} &= y_0, \\ \lambda_3 z_0^{[0]} + o(2) &= 0, \end{aligned} \tag{8}$$

where x_0 and y_0 are undetermined initial values.

3.3. Global matching of the local expansion

The global approximants for the homoclinic orbits are similar to the form of solution at $t \to \pm\infty$ and also meet the nature of the solution at $t \to \pm 0$. The global approximants are analytically expressed, so they can be expanded in power series in the neighborhood of $t = 0$ and then matched directly with the homoclinic series of Eq. (6). As $t \to \pm 0$, the positive and negative approximants $x^{[+]}(t)$ and $x^{[-]}(t)$ are expanded in power series and equated to the corresponding local homoclinic expansion $x^{[0]}(t)$, such as $x^{[\pm]}(t) \approx x^{[0]}(t)$. The Padé approximation method is introduced into the calculation of the following. It has played a role in establishing the relations between the two manifold expressions and solution in the neighborhood of initial value. It gives

$$a_0 + \left(\sum_{p=0} \frac{(\lambda_1 t)^p}{p!} \right) \left(a_1 + a_2 \sum_{q=0} \frac{(\lambda_1 t)^q}{q!} \right.$$

$$+\cdots+a_n\sum_{q=0}\frac{[(n-1)\lambda_1 t]^q}{q!}\Bigg)$$
$$\approx x_0^{[0]}+x_1^{[0]}t+x_2^{[0]}t^2+\cdots. \quad (9)$$

Matching the coefficients of respective powers of t, the coefficients $a_1,\cdots,a_n$ are evaluated in terms of $x_i^{[0]}$ listed as follows:

$$\begin{Bmatrix} a_1\\ a_2\\ \cdots\\ a_n\end{Bmatrix}=\begin{bmatrix} 1 & 1 & \cdots & 1\\ \lambda_1 & 2\lambda_1 & \cdots & n\lambda_1\\ \cdots & \cdots & & \cdots\\ \lambda_1^{n-1} & (2\lambda_1)^{n-1} & \cdots & (n\lambda_1)^{n-1}\end{bmatrix}^{-1}\times\begin{Bmatrix} x_0^{[0]}\\ 1!x_1^{[0]}\\ \cdots\\ (n-1)!x_{n-1}^{[0]}\end{Bmatrix}. \quad (10)$$

Similarly, the 2D manifold equation is obtained as

$$a_{0,0}+\left(\sum_{p=0}\frac{(\lambda_2 t)^p}{p!}\right)\Bigg(a_{1,0}+\cdots+a_{n,0}\sum_{q=0}\frac{[(n-1)\lambda_2 t]^q}{q!}+a_{0,1}\sum_{q=0}\frac{[(\lambda_3-\lambda_2)t]^q}{q!}+\cdots+a_{0,n}\sum_{q=0}\frac{[(n\lambda_3-\lambda_2)t]^q}{q!}$$
$$+a_{1,1}\sum_{q=0}\frac{[\lambda_3 t]^q}{q!}+\cdots+a_{n-1,1}\sum_{q=0}\frac{([(n-2)\lambda_2+\lambda_3]t)^q}{q!}+a_{1,n-1}\sum_{q=0}\frac{[(n-1)\lambda_3 t]^q}{q!}\Bigg)$$
$$\approx x_0^{[0]}+x_1^{[0]}t+x_2^{[0]}t^2+\cdots. \quad (11)$$

The above equations can be simplified into

$$\begin{Bmatrix} a_{1,0}\\ a_{2,0}\\ \cdots\\ a_{n,0}\\ a_{0,1}\\ a_{0,2}\\ \cdots\\ a_{0,n}\\ a_{1,1}\\ a_{1,2}\\ a_{2,1}\\ \cdots\\ a_{n-1,1}\end{Bmatrix}_{1\times s}=\begin{bmatrix} A & B & C\end{bmatrix}_{s\times s}^{-1}\begin{Bmatrix} x_0^{[0]}\\ 1!x_1^{[0]}\\ \cdots\\ (s-1)!x_{(s-1)}^{[0]}\end{Bmatrix}_{1\times s}, \quad (12)$$

where

$$A=\begin{bmatrix} 1 & & \cdots & 1\\ \lambda_2 & 2\lambda_2 & \cdots & n\lambda_2\\ & & \cdots & \\ \lambda_2^{s-1} & (2\lambda_2)^{s-1} & \cdots & (n\lambda_2)^{s-1}\end{bmatrix}_{n\times s};\quad B=\begin{bmatrix} 1 & & \cdots & 1\\ \lambda_3 & 2\lambda_3 & \cdots & n\lambda_3\\ & & \cdots & \\ \lambda_3^{s-1} & (2\lambda_3)^{s-1} & \cdots & (n\lambda_3)^{s-1}\end{bmatrix}_{n\times s};$$
$$C=\begin{bmatrix} 1 & & & \cdots & 1\\ (\lambda_2+\lambda_3) & (\lambda_2+2\lambda_3) & (2\lambda_2+\lambda_3) & \cdots & [(n-1)\lambda_2+\lambda_3]\\ & & & \cdots & \\ (\lambda_2+\lambda_3)^{s-1} & (\lambda_2+2\lambda_3)^{s-1} & (2\lambda_2+\lambda_3)^{s-1} & \cdots & [(n-1)\lambda_2+\lambda_3]^{s-1}\end{bmatrix}_{\frac{n(n-1)}{2}\times s};\quad s=\frac{n(n+3)}{2}. \quad (13)$$

The coefficients of the x in the above equations can be computed in terms of unknown initial conditions. Similar evaluations are carried out for the coefficients of the approximants for y and z. Equations (9) and (11) can be summarized and written in a more general style as

$$\xi_{n_k^{\pm}}^{\pm}=\mathrm{e}^{\mu_k^{\pm}t}(\tau_{k0}^{\pm}\mathrm{e}^{\phi_{k0}^{\pm}t}+\tau_{k1}^{\pm}\mathrm{e}^{\phi_{k1}^{\pm}t}+\cdots+\tau_{kn_k^{\pm}}^{\pm}\mathrm{e}^{\phi_{kn_k^{\pm}}^{\pm}t}). \quad (14)$$

In Eq. (14), $\xi\equiv x$, y, or z, and $n_k^{\pm}$ denotes the number of terms included in the series of $\xi^{\pm}$, $\tau_{ki}^{\pm}$, $\mu_k^{\pm}$, and $\phi_k^{\pm}$ are constants, and their specific expressions are determined by the left terms of Eqs. (9) and (11). Also, a_0 and $a_{0,0}$ are the component values of system at the singular point, namely zero. Approximants with superscript $+(-)$ are termed positive (negative) approximants and are valid only for non-negative (non-positive) values of t. When the orders of approximants on both sides of the equation are taken to be identical, the required numbers of terms are different for 1D and 2D equation. The exponents appearing in the positive and negative approximants are identical to those of the asymptotic expansions in Eqs. (4) and (5) for $t>0$ and $t<0$ respectively. The order of the exponents in Eq. (14) is identical to that in the corresponding local asymptotic expansion. For example, taking the second-order approximant of Eq. (14), the powers are λ_1-th and $2\lambda_1$-th for the 1D equation; the powers are λ_2-th, $2\lambda_2$-th, λ_3-th, $2\lambda_3$-th, and $(\lambda_2+\lambda_3)$-th for the 2D equation. The exponents of the positive and negative approximants are listed in Table 1.

Considering the leading-order terms in the approximants of Eq. (14) and the local expansions of Eqs. (4) and (5), and bringing them back to the original equation, we obtain the following matching conditions when $t\to\pm\infty$:

$$\lambda_1 a_1-b_1=0,$$
$$\lambda_2 a_{1,0}-b_{1,0}=0,$$

$$c_1 + \frac{1}{\lambda_1} a_1 = 0. \tag{15}$$

Table 1. Numbers of terms included in each iteration.

Iteration no.	n_k^+	n_k^-
1	1	2
2	2	5
3	3	9

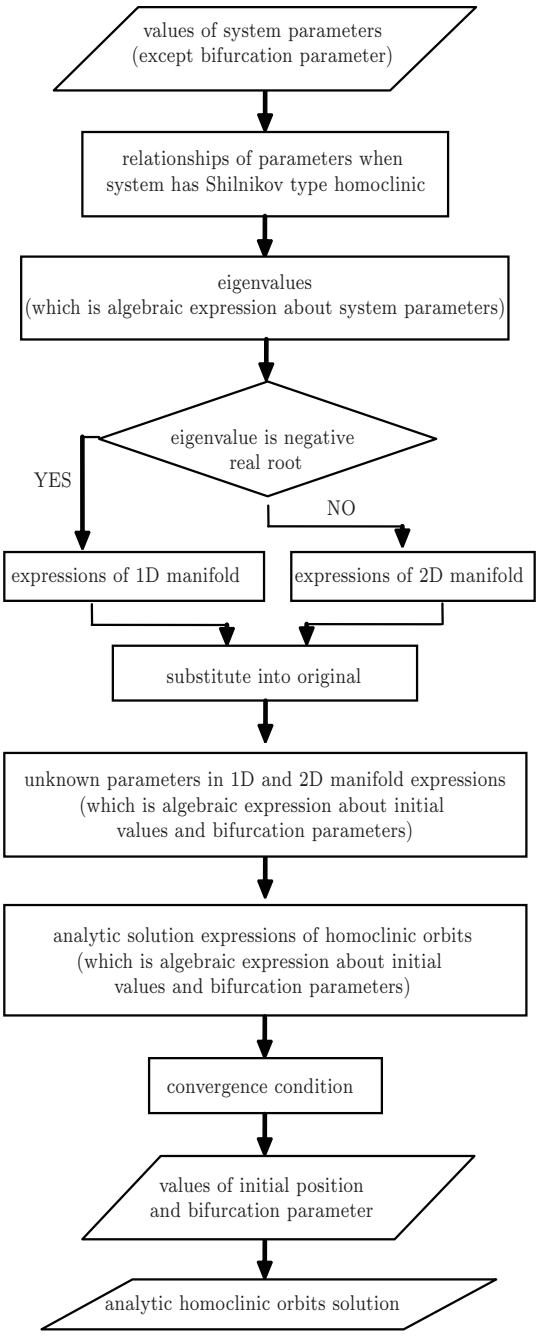


Fig. 4. Procedure structure diagram.

In simultaneous equations (7), (8), (10), (12), (13), and (15), to make any of parameters $\lambda_{1,2,3}$ the bifurcation parameter, and other parameter values are known, the initial point position and the value of bifurcation parameter are obtained directly. Because the coefficients include complex, and the homoclinic solution in negative direction can be written in the following form:

$$\begin{aligned}
x^{[-]}(t) &= \sum_{i=0}^{n}\sum_{j=0}^{n-i}\{\mathrm{Re}(a_{i,j})\cos[\mathrm{Im}(i\lambda_2 t + j\lambda_3 t)] + \\
&\quad \mathrm{Im}(a_{i,j})\sin[\mathrm{Im}(i\lambda_2 t + j\lambda_3 t)]\}\,\mathrm{e}^{\mathrm{Re}(i\lambda_2 t + j\lambda_3 t)}, \\
y^{[-]}(t) &= \sum_{i=0}^{n}\sum_{j=0}^{n-i}\{\mathrm{Re}(b_{i,j})\cos[\mathrm{Im}(i\lambda_2 t + j\lambda_3 t)] + \\
&\quad \mathrm{Im}(b_{i,j})\sin[\mathrm{Im}(i\lambda_2 t + j\lambda_3 t)]\}\,\mathrm{e}^{\mathrm{Re}(i\lambda_2 t + j\lambda_3 t)}, \\
y^{[-]}(t) &= \sum_{i=0}^{n}\sum_{j=0}^{n-i}\{\mathrm{Re}(c_{i,j})\cos[\mathrm{Im}(i\lambda_2 t + j\lambda_3 t)] + \\
&\quad \mathrm{Im}(c_{i,j})\sin[\mathrm{Im}(i\lambda_2 t + j\lambda_3 t)]\}\,\mathrm{e}^{\mathrm{Re}(i\lambda_2 t + j\lambda_3 t)}.
\end{aligned} \tag{16}$$

The above calculation of homoclinic orbits can be achieved by programming. By entering the initial conditions (values of all system parameters except bifurcation parameter), the values of initial position and bifurcation parameter when system has homoclinic orbit can be gained directly, and then the analytic homoclinic solution is obtained by taking advantage of the program. The procedure structural diagram is shown in Fig. 4.

4. Examples

In the traditional method, the first step is to use numerical methods to determine when the homoclinic orbit appears, followed by the calculation process. However, in this paper, we can directly obtain the values of the bifurcation parameter and initial point position by the method presented here.

4.1. Homoclinic orbit of PID controller model

From

$$\begin{aligned}
\dot{x} &= y + \rho xz, \\
\dot{y} &= z + \nu xy, \\
\dot{z} &= -\alpha x - \beta y - \gamma z + \delta x^2 + \kappa x^3,
\end{aligned} \tag{17}$$

the existence of the homoclinic orbit in this system has been rigorously proved as mentioned before.[26] Similarly, the analytic homoclinic orbit in the system is directly solved by the method presented in this paper.

According to the theory of ordinary differential equations, equation (17) has five equilibrium points, which are not listed here because our main concern is the calculation process of the presented method that is used to construct the Shilnikov type homoclinic orbit. The equilibrium point $(0,0,0)$ is only discussed and used in the Jacobian matrix

$$A = \begin{bmatrix} 0 & 1 & 0 \\ 0 & 0 & 1 \\ -\alpha & -\beta & -\gamma \end{bmatrix}. \tag{18}$$

The characteristic polynomial is

$$\lambda^3+\gamma\lambda^2+\beta\lambda+\alpha=0. \tag{19}$$

According to the Cardano formula, it yields

$$\begin{aligned}&\Delta=\left(\frac{m}{2}\right)^2+\left(\frac{n}{3}\right)^2>0,\\&\sqrt[3]{-\frac{n}{2}+\sqrt{\Delta}}-\sqrt[3]{\frac{n}{2}+\sqrt{\Delta}}<\min\left(-\frac{2\gamma}{3},\frac{\gamma}{3}\right),\\&m=\beta-\frac{\gamma^2}{3},\quad n=\alpha-\frac{\beta\gamma}{3}+\frac{2\gamma^3}{27}.\end{aligned} \tag{20}$$

Equation (19) has one real root r and a conjugate pair of complex roots $g\pm\mathrm{i}f$. Here, the real root is negative and the real parts of the complex conjugate roots are both positive. According to the above conditions, we redefine that h, g, $f\in\Re$, $h>0$, $g>0$, $f>0$. A negative real root and a pair of positive real parts of the conjugate complex roots are obtained as

$$\begin{aligned}\lambda_1&=-h,\\\lambda_{2,3}&=g\pm\mathrm{i}f,\end{aligned} \tag{21}$$

see Eq. (A1). Using the presented method as shown in Eq. (7), the following recursive expressions are obtained and represented by the constant coefficients of the series

$$\begin{aligned}x_{k+1}^{[0]}&=\frac{1}{k+1}(y_k^{[0]}+\rho x_k^{[0]}z_k^{[0]}),\\y_{k+1}^{[0]}&=\frac{1}{k+1}(z_k^{[0]}+\nu x_k^{[0]}y_k^{[0]}),\\z_{k+1}^{[0]}&=\frac{1}{k+1}(-\alpha x_k^{[0]}-\beta y_k^{[0]}-\gamma z_k^{[0]}+\delta\sum_{m=0}^{k}\sum_{n=0}^{k-m}x_m^{[0]}x_n^{[0]}\\&\quad+\kappa\sum_{m=0}^{k}\sum_{n=0}^{k-m}\sum_{h=0}^{k-m-n}x_m^{[0]}x_n^{[0]}x_h^{[0]}).\end{aligned} \tag{22}$$

And then the initial conditions are

$$\begin{aligned}x_0^{[0]}&=x_0,\\y_0^{[0]}&=y_0,\\z_0^{[0]}&=\frac{-\alpha x_0+\delta x_0^2+\kappa x_0^3-\beta y_0}{\gamma}.\end{aligned} \tag{23}$$

The results of second and third iteration approximation are listed in Tables A1 and A2, and the initial values are $x_0=0.74656$, $y_0=0.218656$, $\beta=2.9166$, and $x_0=0.745216$, $y_0=0.409924$, $\beta=2.00035$, in which β is the bifurcation parameter and other parameters are chosen to be $\alpha=2.1$, $\gamma=0.45$, $\delta=1$, $\kappa=3.3$, $\rho=0.05$, and $\nu=0.07$. The time series of trajectories $x(t)$, $y(t)$, and $z(t)$ are shown in Fig. 5, and the 3D phase diagram is shown in Fig. 6.

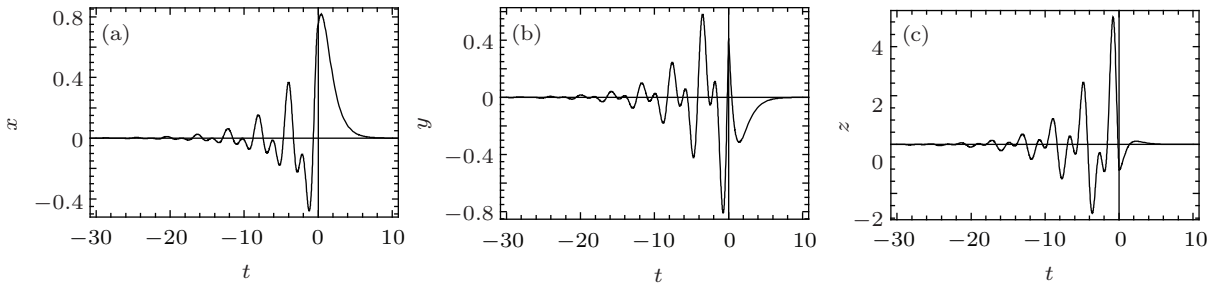


Fig. 5. Time series of the trajectories of the PID controller model: (a) $x(t)$, (b) $y(t)$, and (c) $z(t)$.

The Shilnikov sense Smale horseshoe chaos is predicted to occur in a range of $0.0646801\le\beta\le4.71283$ in terms of the Shilnikov theorem. By using numerical methods, which gradually reduce the value of the parameter β, the evolution process of vibrations can be achieved from a single circle to the first period doubling bifurcation, and then to the second period doubling bifurcation until chaos appears, and the whole evolution process is shown in Fig. 7. When $\beta=2$, analysis reveals that the maximum Lyapunov exponent ($l_1=0.114238$) is greater than zero and meets the exponential requirements for a chaotic attractor; the Hausdorff dimension is 2.08259 which verifies that chaotic motion occurs. The projections of the chaotic attractor on (x–y), (y–z), and (x–z) planes are shown in Fig. 8. We can see that the value of chaotic bifurcation parameter with the third iteration approximation $\beta=2.00035$ is very close to the one with numerical method $\beta=2$. Compared with the results obtained by applying the Shilnikov theorem, the range of bifurcation parameter determined by the presented method is more accurate when the Shilnikov type chaotic motion in a 3D system occurs. And for the method, generally speaking, according to the calculation experience the third iteration approximation has remarkably high accuracy.

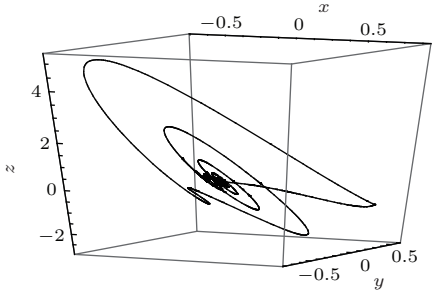


Fig. 6. The 3D phase diagram of the PID controller model.

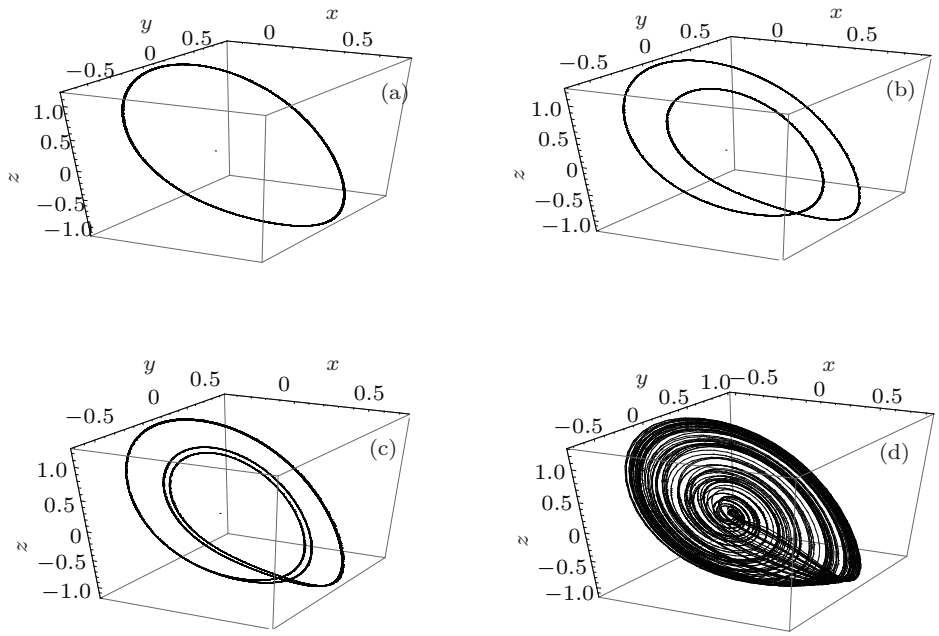


Fig. 7. The process of periodic doubling bifurcation and the chaotic phase diagram with: (a) $\beta = 2.2$, (b) $\beta = 2.096$, (c) $\beta = 2.089$, and (d) $\beta = 2$.

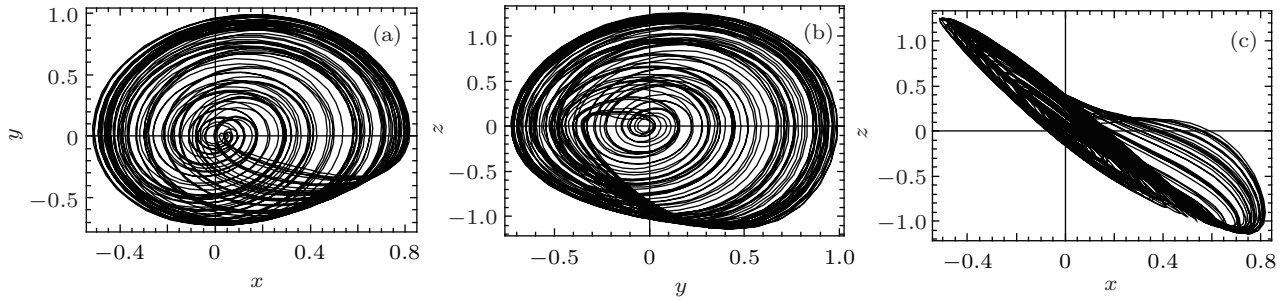


Fig. 8. Projections of the chaotic attractor on (a) (x–y), (b) (y–z), and (c) (x–z) planes.

4.2. Homoclinic orbit of a simplified WINDMI model

From

$$\begin{aligned}\dot{x} &= -y,\\ \dot{y} &= \alpha x - \kappa y - z,\\ \dot{z} &= -\beta - \gamma \tanh\left[x - \operatorname{artanh}\left(\frac{\beta}{\gamma}\right)\right],\end{aligned} \tag{24}$$

the existence of a homoclinic orbit in this system has also been rigorously proved.[26] Similarly, the analytic homoclinic orbits and bifurcation parameter in the system are directly solved. In a similar way to the process in last part, we redefine h, g, $f \in \Re$, $h > 0$, $g > 0$, $f > 0$ at the origin $(0,0,0)$, which is one of the equilibrium points. A negative real root and a pair of positive real parts of the conjugate complex roots are obtained as follows:

$$\begin{aligned}\lambda_1 &= -h,\\ \lambda_{2,3} &= g \pm \mathrm{i} f,\end{aligned} \tag{25}$$

see Appendix (A2). The results of the second and third iteration approximations can be obtained on the basis of the method used in the previous section; so the results are not listed here. The third iteration is shown in Table A3, the initial values are $x_0 = -0.216472$, $y_0 = 0.77731$, $\beta = 0.8000$, in which β is the bifurcation parameter and other parameters are chosen to be $\alpha = 1.45$, $\beta = 28$, and $\gamma = 30$. The time series of trajectories $x(t)$, $y(t)$, and $z(t)$ are shown in Fig. 9. and the 3D phase diagram is shown in Fig. 10.

Being similar to the analysis results in the previous section, the Shilnikov sense Smale horseshoe chaos is predicted to occur in a range of $0 \leq \beta \leq 2.08567$ by applying the Shilnikov theorem. When $\beta = 0.8$, analysis reveals that the maximum Lyapunov exponent ($l_1 = 0.11341$) is greater than zero and meets the exponential requirements for a chaotic attractor; the Hausdorff dimension is 2.1265 which verifies that the chaotic motion occurs. The value of chaotic bifurcation parameter with the third iteration approximation $\beta = 0.80001$ is very close to the one with numerical method $\beta = 0.8$. Again, it is proved that presented method is an effective method.

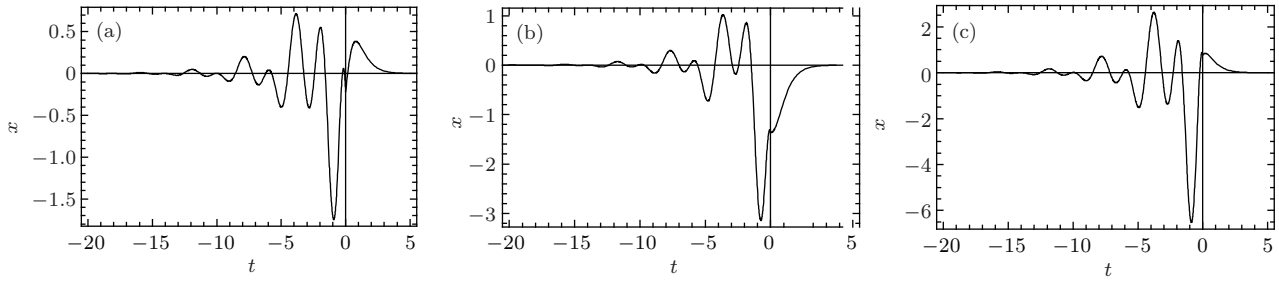


Fig. 9. Time series of trajectories of the simplified WINDMI model. (a) $x(t)$, (b) $y(t)$, and (c) $z(t)$.

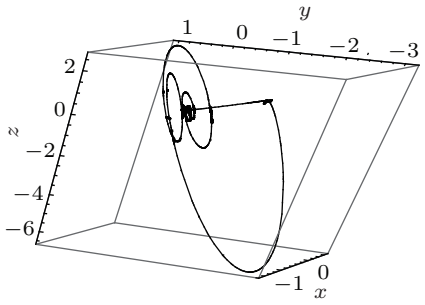


Fig. 10. The 3D phase diagram of the simplified WINDMI model.

4.3. Homoclinic orbit of a human DNA sequences model

The low-dimensional nonlinear dynamical system serving as a human DNA sequence model is obtained when large-scale nucleotide compositional fluctuations of the human genome are explored. The observed nonlinear oscillations are likely to display all the characteristic features of chaotic strange attractors, which suggest a very attractive deterministic picture: gene orientation and location are related to the structure and dynamics of chromation. The third-order nonlinear ordinary differential equation is

$$\dddot{\theta} + \alpha\ddot{\theta} + \beta\dot{\theta} + \gamma\theta + \kappa\theta^3 = 0, \tag{26}$$

which has been emphasized to be the paradigm of nonlinear oscillators that display homoclinic chaos of Shilnikov type.[27,28] When adjusting the values ($\alpha = -5.5$, $\beta = 3.5$, $\gamma = 1$, $\kappa = 1$) of parameters close to those under homoclinic conditions, it is possible to observe the spiraling strange attractor behavior that is intermittently reinjected to the neighbourhood of the saddle focus. This is located at the origin after some oscillations around the two other saddle foci, which ensures the nonlinear saturation of the dynamics. Homoclinic orbits and Shilnikov homoclinic chaos of system (26) have been obtained through numerical methods.[29]

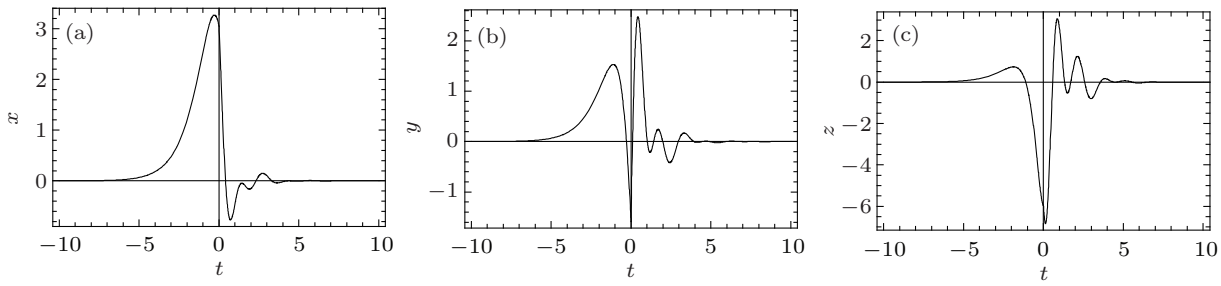


Fig. 11. Time series of trajectories of a human DNA sequences model: (a) $x(t)$, (b) $y(t)$, and (c) $z(t)$.

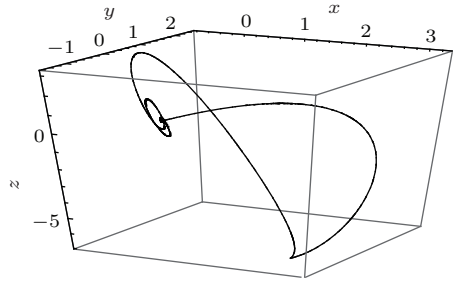


Fig. 12. The 3D phase diagram of a human DNA sequences model.

At this stage, the homoclinic orbits and homoclinic bifurcation of system (26) are investigated with the analytical method presented in this article. Thus, system (26) can be written in the following form:

$$\begin{aligned} \dot{x} &= y, \\ \dot{y} &= z, \\ \dot{z} &= -\gamma x - \beta y - \alpha z - \kappa x^3. \end{aligned} \tag{27}$$

The existence of homoclinic chaos has been verified in Ref. [29], and the main attention should be paid to the analytic homoclinic orbit and the more accurate critical value of chaos. According to the previous process, we redefine $h, g, f \in \Re, h > 0, g > 0, f > 0$ at the origin $(0,0,0)$, which is one of the equilibrium points. A negative real root and a pair of positive real parts of the conjugate complex roots are

obtained as

$$\lambda_1 = -h,$$
$$\lambda_{2,3} = g \pm \mathrm{i} f, \tag{28}$$

see Eq. (A3). Let β be the bifurcation parameter and other parameters are chosen to be those mentioned previously, i.e., $\alpha = -5.5$, $\gamma = 1$, and $\kappa = 1$, and the initial values are taken to be $x_0 = 3.04493$, $y_0 = -1.58321$, and $\beta = 3.49145$, the results of the second and third iteration approximation are almost the same, so the second iteration is listed in Table A4 but the results of the third iteration approximation are not presented here. The value of chaotic bifurcation parameter with the second iteration approximations $\beta = 3.49145$ is very close to the one with numerical method $\beta = 3.5$. In contrast, the Shilnikov sense Smale horseshoe chaos is predicted to occur in a range of $0 \le \beta \le 4.78315$ by applying Shilnikov theorem. The presented method is proved to be effective. The time series of trajectories $x(t)$, $y(t)$, and $z(t)$ are shown in Fig. 11 and the 3D phase diagram is displayed in Fig. 12.

5. Conclusion

In this article, the problem of Shilnikov sense Smale horseshoe chaos in a 3D system is studied. It is known that the existence of homoclinic orbits is proved from a mathematical point of view, but the descriptions of orbital analytic expression are lacking in the existing literature. Hence, in this paper, we present a method to construct the analytical expression of Shilnikov-type homoclinic orbits. Additionally, more accurate ranges of values of bifurcation parameter and initial point position are obtained directly when the system has homoclinic orbits. The Padé approximation method and analytic solution in the neighborhood of initial value are introduced into the calculation of the series expressions of the stable and unstable manifolds of the saddle-focus equilibrium, which has some advantages such as expanding the scope of application, improving the accuracy of the solution, and avoiding the computational complexity caused by higher-order response.

The strategy presented in this work is generally applied and accepted. Hence, it would be possible to apply the presented method to research other 3D systems with more complicated nonlinearity, which will be a topic for the further study.

Appendix A

$$\begin{aligned}
h =\ & [6\times 2^{1/3}\beta - 2\times 2^{1/3}\gamma^2 + 2\gamma(-27\alpha + 9\beta\gamma - 2\gamma^3 + 3\sqrt{3}\sqrt{27\alpha^2 + 4\beta^3 - 18\alpha\beta\gamma - \beta^2\gamma^2 + 4\alpha\gamma^3})^{1/3} \\
& - (-54\alpha + 18\beta\gamma - 4\gamma^3 + 6\sqrt{3}\sqrt{27\alpha^2 + 4\beta^3 - 18\alpha\beta\gamma - \beta^2\gamma^2 + 4\alpha\gamma^3})^{2/3}]/ \\
& [6(-27\alpha + 9\beta\gamma - 2\gamma^3 + 3\sqrt{3}\sqrt{27\alpha^2 + 4\beta^3 - 18\alpha\beta\gamma - \beta^2\gamma^2 + 4\alpha\gamma^3})^{1/3}], \\
g =\ & [6\times 2^{1/3}\beta - 2\times 2^{1/3}\gamma^2 - 4\gamma(-27\alpha + 9\beta\gamma - 2\gamma^3 + 3\sqrt{3}\sqrt{27\alpha^2 + 4\beta^3 - 18\alpha\beta\gamma - \beta^2\gamma^2 + 4\alpha\gamma^3})^{1/3} \\
& - (-54\alpha + 18\beta\gamma - 4\gamma^3 - 6\sqrt{3}\sqrt{27\alpha^2 + 4\beta^3 - 18\alpha\beta\gamma - \beta^2\gamma^2 + 4\alpha\gamma^3})^{2/3}]/ \\
& [12(-27\alpha + 9\beta\gamma - 2\gamma^3 + 3\sqrt{3}\sqrt{27\alpha^2 + 4\beta^3 - 18\alpha\beta\gamma - \beta^2\gamma^2 + 4\alpha\gamma^3})^{1/3}], \\
f =\ & [6\beta - 2\gamma^2 + 2^{1/3}(-27\alpha + 9\beta\gamma - 2\gamma^3 + +3\sqrt{3}\sqrt{27\alpha^2 + 4\beta^3 - 18\alpha\beta\gamma - \beta^2\gamma^2 + 4\alpha\gamma^3})^{2/3}/ \\
& [2\times 2^{2/3}\sqrt{3}(-27\alpha + 9\beta\gamma - 2\gamma^3 + 3\sqrt{3}\sqrt{27\alpha^2 + 4\beta^3 - 18\alpha\beta\gamma - \beta^2\gamma^2 + 4\alpha\gamma^3})^{1/3}].
\end{aligned} \tag{A1}$$

$$\begin{aligned}
h =\ & [6\times 2^{1/3}\alpha\gamma^2 - 2\times 2^{1/3}\gamma^2\kappa^2 + 2\gamma\kappa(27\beta^2\gamma^2 - 27\gamma^4 + 9\alpha\gamma^3\kappa - 2\gamma^3\kappa^3 \\
& + \sqrt{4\gamma^6(3\alpha - \kappa^2)^3 + \gamma^4[27\beta^2 + \gamma(-27\gamma + 9\alpha\kappa - 2\kappa^3)]^2})^{1/3} - 2^{2/3}(27\beta^2\gamma^2 - 27\gamma^4 + 9\alpha\gamma^3\kappa - 2\gamma^3\kappa^3 \\
& \sqrt{4\gamma^6(3\alpha - \kappa^2)^3 + \gamma^4[27\beta^2 + \gamma(-27\gamma + 9\alpha\kappa - 2\kappa^3)]^2})^{2/3}]/[6\gamma(27\beta^2\gamma^2 - 27\gamma^4 + 9\alpha\gamma^3\kappa - 2\gamma^3\kappa^3 \\
& + \sqrt{4\gamma^6(3\alpha - \kappa^2)^3 + \gamma^4[27\beta^2 + \gamma(-27\gamma + 9\alpha\kappa - 2\kappa^3)]^2})^{1/3}], \\
g =\ & [6\times 2^{1/3}\alpha\gamma^2 - 2\times 2^{1/3}\gamma^2\kappa^2 - 4\gamma\kappa(27\beta^2\gamma^2 - 27\gamma^4 + 9\alpha\gamma^3\kappa - 2\gamma^3\kappa^3 \\
& + \sqrt{4\gamma^6(3\alpha - \kappa^2)^3 + \gamma^4[27\beta^2 + \gamma(-27\gamma + 9\alpha\kappa - 2\kappa^3)]^2})^{1/3} \\
& - 2^{2/3}(27\beta^2\gamma^2 - 27\gamma^4 + 9\alpha\gamma^3\kappa - 2\gamma^3\kappa^3 + \sqrt{4\gamma^6(3\alpha - \kappa^2)^3 + \gamma^4[27\beta^2 + \gamma(-27\gamma + 9\alpha\kappa - 2\kappa^3)]^2})^{2/3}]/ \\
& [12\gamma(27\beta^2\gamma^2 - 27\gamma^4 + 9\alpha\gamma^3\kappa - 2\gamma^3\kappa^3 + \sqrt{4\gamma^6(3\alpha - \kappa^2)^3 + \gamma^4[27\beta^2 + \gamma(-27\gamma + 9\alpha\kappa - 2\kappa^3)]^2})^{1/3}],
\end{aligned}$$

$$
\begin{aligned}
f &= [6\alpha\gamma^2 - 2\gamma^2\kappa^2 + 2^{1/3}(27\beta^2\gamma^2 - 27\gamma^4 + 9\alpha\gamma^3\kappa - 2\gamma^3\kappa^3 + \sqrt{4\gamma^6(3\alpha-\kappa^2)^3 + \gamma^4[27\beta^2 + \gamma(-27\gamma + 9\alpha\kappa - 2\kappa^3)]^2})^{2/3}]/ \\
&\quad [2\times 2^{2/3}\sqrt{3}\gamma(27\beta^2\gamma^2 - 27\gamma^4 + 9\alpha\gamma^3\kappa - 2\gamma^3\kappa^3 + \sqrt{4\gamma^6(3\alpha-\kappa^2)^3 + \gamma^4[27\beta^2 + \gamma(-27\gamma + 9\alpha\kappa - 2\kappa^3)]^2})^{1/3}]. \qquad \text{(A2)} \\
h &= [6\times 2^{1/3}\beta - 2\times 2^{1/3}\gamma^2 + 2\gamma(-27\alpha + 9\beta\gamma - 2\gamma^3 + 3\sqrt{3}\sqrt{27\alpha^2 + 4\beta^3 - 18\alpha\beta\gamma - \beta^2\gamma^2 + 4\alpha\gamma^3})^{1/3} \\
&\quad - (-54\alpha + 18\beta\gamma - 4\gamma^3 + 6\sqrt{3}\sqrt{27\alpha^2 + 4\beta^3 - 18\alpha\beta\gamma - \beta^2\gamma^2 + 4\alpha\gamma^3})^{2/3}]/ \\
&\quad [6(-27\alpha + 9\beta\gamma - 2\gamma^3 + 3\sqrt{3}\sqrt{27\alpha^2 + 4\beta^3 - 18\alpha\beta\gamma - \beta^2\gamma^2 + 4\alpha\gamma^3})^{1/3}], \\
g &= [6\times 2^{1/3}\beta - 2\times 2^{1/3}\gamma^2 - 4\gamma(-27\alpha + 9\beta\gamma - 2\gamma^3 + 3\sqrt{3}\sqrt{27\alpha^2 + 4\beta^3 - 18\alpha\beta\gamma - \beta^2\gamma^2 + 4\alpha\gamma^3})^{1/3} \\
&\quad - (-54\alpha + 18\beta\gamma - 4\gamma^3 + 6\sqrt{3}\sqrt{27\alpha^2 + 4\beta^3 - 18\alpha\beta\gamma - \beta^2\gamma^2 + 4\alpha\gamma^3})^{2/3}]/ \\
&\quad [12(-27\alpha + 9\beta\gamma - 2\gamma^3 + 3\sqrt{3}\sqrt{27\alpha^2 + 4\beta^3 - 18\alpha\beta\gamma - \beta^2\gamma^2 + 4\alpha\gamma^3})^{1/3}], \\
f &= [6\beta - 2\gamma^2 + 2^{1/3}(-27\alpha + 9\beta\gamma - 2\gamma^3 + 3\sqrt{3}\sqrt{27\alpha^2 + 4\beta^3 - 18\alpha\beta\gamma - \beta^2\gamma^2 + 4\alpha\gamma^3})^{2/3}/ \\
&\quad [2\times 2^{2/3}\sqrt{3}(-27\alpha + 9\beta\gamma - 2\gamma^3 + 3\sqrt{3}\sqrt{27\alpha^2 + 4\beta^3 - 18\alpha\beta\gamma - \beta^2\gamma^2 + 4\alpha\gamma^3})^{1/3}]. \qquad \text{(A3)}
\end{aligned}
$$

Table A1. Parameters gained from the second iteration approximation.

n_k	$\tau^+_{xn_k}$	$\tau^+_{yn_k}$	$\tau^+_{zn_k}$	$\tau^-_{xn_k}$	$\tau^-_{yn_k}$	$\tau^-_{zn_k}$
1	2.30709	–1.5704	1.07389	$0.0985956 - 0.0271714i$	0.059147+0.164868i	–0.437029+0.12153i
2	–2.08768	2.91838	–3.98135	0.00135552+0.00715758i	–0.0199643+0.00855898i	$0.00349617 - 0.0665576i$
3	0.527149	–1.12933	2.29627	0.0985958+0.0271714i	$0.059147 - 0.164868i$	$-0.437029 - 0.12153i$
4				$0.00135552 - 0.00715758i$	$-0.0199643 - 0.00855898i$	0.00349617+0.0665576i
5				0.546658	0.14029	0.255875

Table A2. Parameters gained from the third iteration approximation.

$\tau^+_{xn_k}$	$\tau^+_{xn_k}$	$\tau^+_{xn_k}$	$\tau^+_{xn_k}$	$\tau^+_{xn_k}$	$\tau^+_{xn_k}$	$\tau^+_{xn_k}$
1	2.85991	–2.48994	2.21493	0.422638+101094i	0.0515778+0.706785i	–1.5295–4.02395i
2	–3.29529	5.89609	–10.3641	0.0175494+0.0134036i	–0.0138408+0.0326742i	–0.43532–0.0793688i
3	1.41297	–3.82731	9.96011	–0.00194746+0.0000151032i	–0.00283419–0.00413389i	0.0373831–0.00649003i
4	–0.232378	0.831085	–2.84174	0.422638–101094i	0.0515778–0.706785i	–1.5295+4.02395i
5				0.0175494–0.0134036i	–0.0138408–0.0326742i	–0.43532+0.0793688i
6				–0.00194746–0.0000151032i	–0.00283419+0.00413389i	0.0373831+0.00649003i
7				0.0975077	0.0526614	3.24923
8				–0.114386+0.228677i	0.143728+0.358839i	–0.212596–4.24787i
9				–0.114386–0.228677i	0.143728–0.358839i	–0.212596+4.24787i

Table A3. Parameters gained from the third iteration approximation.

n	a_n	b_n	c_n	$a_{i,j}$	$b_{i,j}$	$c_{i,j}$
1	2.96183	–4.4999	2.37494	1.6608+0.775016i	1.56335+2.05309i	5.2051+3.60345i
2	–7.04335	5.59472	–1.6409	0.0984714–0.0926163i	0.267217–0.124596i	0.278282–0.605075i
3	5.23268	–3.14569	–0.280456	–0.00651632+0.00265007i	–0.0118798+0.00150179i	–0.0265188+0.0177963i
4	–1.36766	0.686887	0.323722	1.6608–0.775016i	1.56335–2.05309i	5.2051–3.60345i
5				0.0984714+0.0926163i	0.267217+0.124596i	0.278282+0.605075i
6				–0.00651632–0.00265007i	–0.0118798–0.00150179i	–0.0265188–0.0177963i
7				–2.88748	–4.12756	–7.1231
8				–0.41733+1.56967i	–0.436907+2.59043i	–1.50666+4.04916i
9				–0.41733–1.56967i	–0.436907–2.59043i	–1.50666–4.04916i

Table A4. Parameters gained from the second iteration approximation.

n_k	$\tau^+_{xn_k}$	$\tau^+_{yn_k}$	$\tau^+_{zn_k}$	$\tau^-_{xn_k}$	$\tau^-_{yn_k}$	$\tau^-_{zn_k}$
1	10.1166	10.1267	10.1369	1.04287–0.561121i	0.146053+2.77206i	–8.03507–2.78053i
2	–9.5167	–19.0526	–38.1435	–0.06742–0.00519073i	0.156914–0.2754444i	1.3196+0.899745i
3	2.44507	7.34261	22.05	1.04287+0.561121i	0.146053–2.77206i	–8.03507+2.78053i
4				–0.06742+0.00519073i	0.156914+0.2754444i	1.3196–0.899745i
5				1.09402	–2.18914	7.47439

References

[1] Lorenz E N 1963 *J. Atmos. Sci.* **20** 130
[2] Ozoguz S, Elwakil A S and Kennedy M P 2002 *Int. J. Bifurc. Chaos* **12** 1627
[3] Rössler O E 1996 *Phys. Lett. A* **57** 397
[4] Chen G and Ueta T 1999 *Int. J. Bifurc. Chaos* **9** 1465
[5] Shilnikov L P 2000 *Homoclinic Orbits: Since Poincaré till Today* **571** WIAS
[6] Uuml J H, Chen G R and Yu Y G 2002 *Chin. Phys. Lett.* **19** 1260
[7] Zhang R, Hu A H and Xu Z Y 2007 *Acta Phys. Sin.* **56** 6851 (in Chinese)
[8] Li Zhi and H C Z 2002 *Chin. Phys* **11** 666
[9] Leonov G A 2001 *J. Appl. Math. Mech.* **65** 19
[10] Li Z, Chen G R and Halang W A 2004 *Inform. Sci.* **165** 235
[11] Genesio R, Innocenti G and Gualdani F 2008 *Phys. Lett. A* **372** 1799
[12] Silva C P 1993 *IEEE Trans. Circuits Syst. Regul. Pap.* **40** 675
[13] Palmer K J 1996 *Nonlinear Anal. Theory Methods Appl.* **27** 1075
[14] Zhang Q C, Tian R L and Wang W 2008 *Acta. Phys. Sin* **57** 2799 (in Chinese)
[15] Zhou T S, Chen G R and Yang Q G 2004 *Chaos, Solitons Fractals* **19** 985
[16] Mikhlin Y V 2000 *J. Sound Vib.* **230** 971
[17] Vakakis A F and Azeez M F A 1998 *Nonlinear Dyn.* **15** 245
[18] Li Y H and Zhu S 2006 *Chaos, Solitons Fractals* **29** 1155
[19] Nandakumar K and Chatterjee A 2008 *Nonlinear Dyn.* **57** 383
[20] Chen B Y, Zhou T S and Chen G R 2009 *Int. J. Bifurc. Chaos* **19** 1679
[21] Emaci E, Vakakis A F, Andrianov I V and Mikhlin Y 1997 *Nonlinear Dyn.* **13** 327
[22] Manucharyan G V and Mikhlin Y V 2005 *J. Appl. Math. Mech.* **69** 39
[23] Mikhlin Y V 1995 *J. Sound Vib.* **182** 577
[24] Feng J J, Zhang Q C and Wang W 2012 *Chaos, Solitons Fractals* **45** 950
[25] Feng J J, Zhang Q C and Wang W 2011 *Chin. Phys. B* **20** 090202
[26] Wang W, Zhang Q C and Tian R L 2010 *Chin. Phys. B* **19** 030517
[27] Arneodo A, Coullet P and Tresser C 1981 *Commun. Math. Phys.* **79** 573
[28] Arneodo A, Coullet P H and Spiegel E A 1985 *Geophys. Astrophys. Fluid Dyn.* **31** 1
[29] Nicolay S, Argoul F, Touchon M, d'aubenton-Carafa Y, Thermes C and Arneodo A 2004 *Phys. Rev. Lett.* **93** 108101